J. Electrochem. Sci. Eng. **15(2)** (2025) 2567; http://dx.doi.org/10.5599/jese.2567

Open Access : : ISSN 1847-9286
https://pub.iapchem.org/ojs/index.php/JESE

Original scientific paper

Machinability studies on metal additive manufactured 316L stainless steel using electrochemical machine

Rajan Natarajan[1,✉], Shanmugapriyan Kanagaraj[1], Thangavel Palaniappan[2] and Deepa Dhanaskodi[3]

[1]*Vinayaka Mission's Kirupananda Variyar Engineering College, Vinayaka Mission's Research Foundation, Deemed to be University, Salem-636308, India*
[2]*Erode Sengunthar Engineering College, Perundurai 638057, India*
[3]*Bannari Amman Institute of Technology, Sathyamangalam, 638401, India*

Corresponding authors: ✉nrajaned@gmail.com

Received: November 12, 2024; Accepted: January 21, 2025; Published: January 30, 2025

Abstract

Metal additive manufactured 316L stainless steel is considered for machinability studies through electrochemical machining (ECM). This material is used in prototyping in the automotive, aerospace, jewellery and biomedical industries, where customized components for individual circumstances are required. In this study, ECM process parameters such as voltage, electrolyte concentration, duty cycle, and selection of an L16 orthogonal array sing four levels were considered for optimization. The multi-criteria decision machining method, namely entropy-based multi-objective optimization, is used for performance analysis based on the ratio analysis method. The study reveals that 14 V, 35 g l^{-1} $NaNO_3$ electrolyte concentration, and 90 % duty cycle are recommended for optimal machining performance. According to the main effect table, the best combination is 16 V, 35 g l^{-1} electrolyte concentration, and 60 % duty cycle. Analysis of variance result shows that the duty cycle accounts for approximately 27.06 1% of machining performance, voltage contributes by 24.015 % and electrolyte content contributes roughly 15.58 % to the machining performance. A scanning electron microscope was used to scan each micromachined hole, and different resolution images were taken in order to analyse the machined hole quality.

Keywords

Additively built austenitic steel; micromachined holes; electrochemical process parameters; multi-objective optimization (MOORA); entropy weighting; variance analysis

Introduction

Metal additive manufacturing (AM) has garnered widespread recognition on a limited range of elemental metals and alloys due to its capacity to produce small quantities at low cost, handle intricate part geometries and optimized topologies, attain moderate part density (>90 %), and demonstrate mechanical performance in uniaxial, biaxial, and torsion testing [1,2]. Masek *et al*. [3] have studied the

effect of milling parameters on the 3D-printed 316 stainless steel (SS). They stated that surface profiles and forces recorded during the machining of the additively built specimen indirectly revealed the variability of the mechanical characteristics. When low cutting conditions were used, the machinability of the additively created specimens improved. In the event of total force and surface roughness, increasing cutting circumstances deteriorate their relative machinability. The cutting reactions of Ti6Al4V alloy that was additively created using solid ceramic tools under dry high-speed milling procedures were investigated by Zhang *et al*. [4] in 2020. As a result of machining parameters, a number of issues were examined, including cutting forces and cutting temperature fields. The findings suggest that feed rate influences temperature fields and cutting force magnitudes more than cutting speed. The machinability of the Inconel 718 superalloy sintered using a direct laser was examined by Chen *et al.* [5] in 2021. The outcomes showed that the coated carbide instruments may be used to cut the LAM Inconel 718 superalloy. Using coated carbide tools, the LAM Inconel 718 superalloy produced cutting forces, temperatures, and vibrations that were approximately 9.63, 6.29, and 16.67 % lower than those of the wrought Inconel 718 superalloy, respectively. The study conducted by Karabulut and Kaynak [6] concentrated on the drilling process of Inconel 718 alloy, which was produced by selective laser melting AM. Using carbide drill bits and varying drilling parameters, such as feed values and cutting speeds, specimens created by selective laser melting (SLM) were drilled. This study demonstrated how surface roughness is decreased throughout the drilling process, improving the surface quality of Inconel 718, which is additively built. Additively manufactured Inconel 625 metal workpieces show significantly unique behaviour on the machinability aspect of the finish milling process. They experienced the tool wear of the inserts, such as edge chipping and coat peeling. They observed that the milling force increases with the cutting speed and feed rate [7]. Bai *et al.* [8] machined directed energy deposition ASTM A131 steel using a milling technique and found that the largest cutting forces were caused by interference between the cutting tool and a significant number of melt-pool barriers, which restrict material flow. Tool wear tends to increase during the machining of the samples. Li *et al*. [9] investigated the machinability of 3D-printed SS316L and reported that the cutting force components Fx and Fy are found to be 76.8 and 48.88 N, respectively. The impact of using a standard grinding procedure on surface roughness and residual stress has been investigated by Ramachandran *et al*. [10] in 2024. High-cycle fatigue mechanical testing was carried out to confirm improved output performance. The surface grinding process is responsible for the noticeable improvement. The aforementioned research makes it clear that machinability tests are conducted on additive manufactured (AMed) components with the goal of enhancing surface and dimension quality. These AMed components are typically surface-ground and machined using traditional production techniques. The inherent drawbacks of this method include high residual stress, excessive tool wear and damage, and increased heat generation at the tool-workpiece interface as a result of the higher mechanical properties of the integrated components. Electrochemical machining (ECM) is used to machine the AM components for holes to get around these issues. Process parameters such as voltage, electrolyte concentration, duty cycle, and selection of an L_{16} orthogonal array (OA) were optimized using four levels of selection. The multi-criteria decision machining method, namely the entropy-based multi-objective optimization based on ratio analysis (MOORA) method, is used performance analysis. The MOORA method was used by Gadakh *et al*. [11] for welding factors optimization, Bhaskar and Khan [12] for dental material selection, Soundarrajan and Thanigaivelan [13] and Vempannan *et al*. [14] for ECM process optimization, and Thiraviam *et al*. [15] for wear parameters analysis. Literature data for the ECM process optimization using entropy and MOORA is generally sparse; hence, in this research, ECM parameters are optimized using this former method. A scanning

electron microscope (SEM) was used to scan each micro-machined hole, and different resolution images were taken to analyse the machined hole quality.

Experimental

High-performance marine-grade austenitic stainless steel with molybdenum alloying for improved corrosion resistance in chloride conditions is called EOS stainless steel 316L. For many uses in the process, energy, paper, transportation, and other sectors, 316L is a standard material. A powdered stainless steel, called EOS stainless steel 316L, is designed to be used in the production of parts using direct metal laser sintering (DMLS) procedure using EOS metal systems. EOS stainless steel 316L is a high-performance metal powder commonly used in additive manufacturing, notably 3D printing procedures like DMLS. It is commonly used to create components that require great strength, corrosion resistance, and longevity. The energy dispersive X-ray spectroscopy (EDAX) tests were performed to check the composition of the specimen EOS stainless steel 316L and revealed that all the alloying materials were present in the expected composition. Figures 1 and 2 show the elements chart and machined as received components EOS stainless steel 316L, respectively. This component was subjected to ECM machinability studies for making micro-holes. Figure 3 shows the setup used for making micro-holes on the EOS stainless steel 316L.

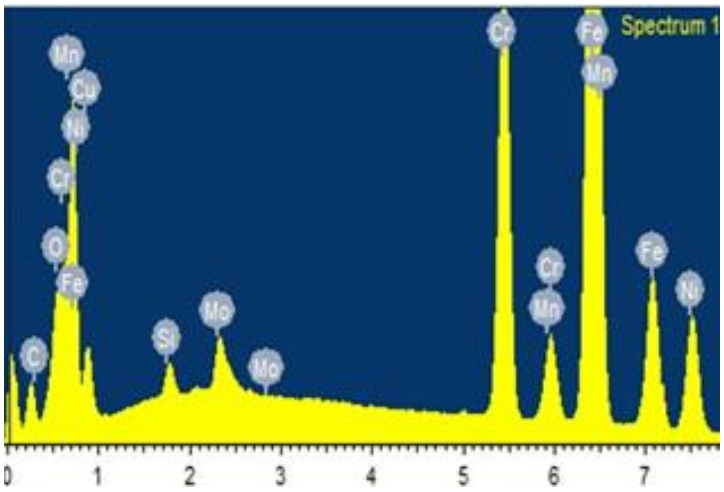

Element	Content, wt.%	Content, at.%
O	5.74	21.56
C	2.14	5.41
Si	0.63	0.99
Cr	16.23	13.77
Mn	1.10	0.88
Fe	61.65	48.69
Ni	9.69	7.28
Cu	0.52	0.36
Mo	2.31	1.06
Total	100.01	100.00

Figure 1. *Elements details of the EOS stainless steel 316L*

(a) (b)

Figure 2. *Machined EOS stainless steel 316L with (a) 7 holes and (b) 9 holes*

The ECM setup consists of a machine structure, machining tank, filter with circulation pump, tool feeders with stepper motor and pulsed power supply [16]. In ECM, the tool electrode, the stitching needle of diameter 460 µm, is connected with a negative power supply, while the workpiece EOS stainless steel 316L is connected with a positive power supply. The tool electrode circumference is insulated with bonding liquid to prevent the stray current. The electrolyte $NaNO_3$ is used to bridge two electrodes, and the pulse power supply initiates and sustains the electrochemical machining process as per Faraday's law of electrolysis [17]. The electrolyte is prepared by mixing different amounts of sodium nitrate salt in 1 l of distilled water. The brine solution is mixed thoroughly with the magnetic stirrer.

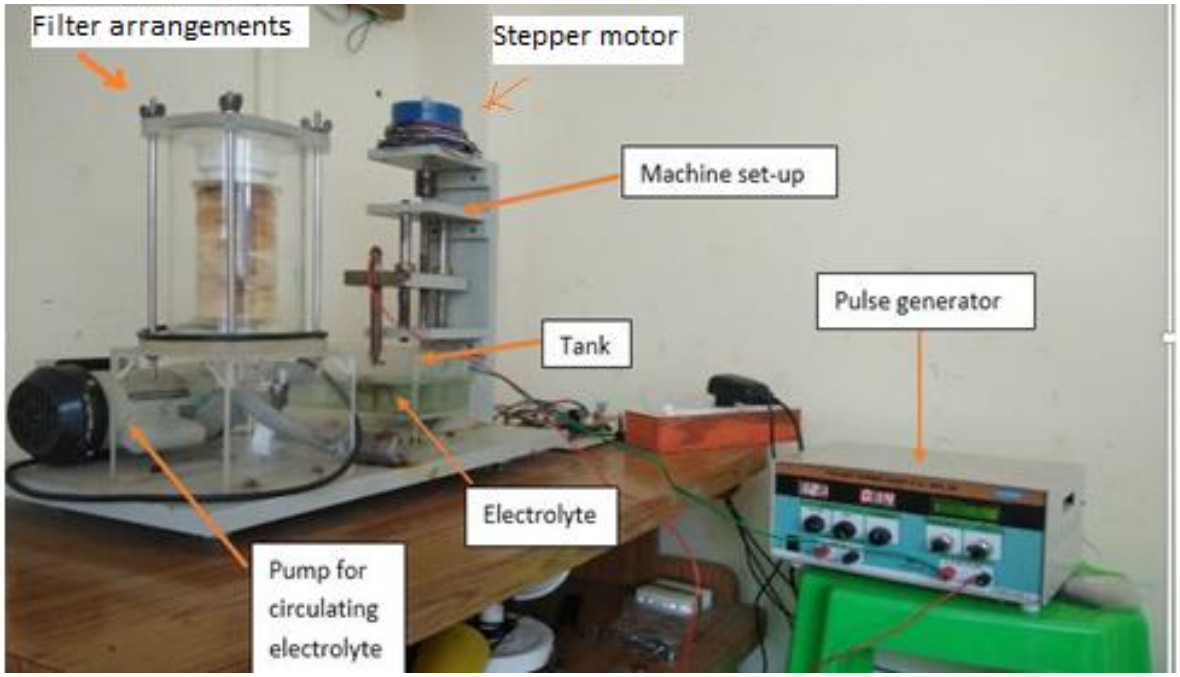

Figure 3. *ECM setup with subsystems*

In this experiment, the ECM process variables, namely voltage, electrolyte concentration and duty cycle, were varied and effects on the material removal rate (MRR) and overcut are followed. L_{16} OA is used for experiments, as presented in Table 1.

Table 1*. L_{16} OA experiment plan*

Exp. No	Voltage, V	$NaNO_3$ electrolyte concentration, g l^{-1}	Duty cycle, %	Material removal rate, mm min^{-1}	Overcut, mm
1	10	30	60	0.0291	0.625
2	10	35	70	0.0306	0.580
3	10	40	80	0.0521	0.349
4	10	45	90	0.0312	0.568
5	12	30	70	0.0320	0.604
6	12	35	60	0.0308	0.567
7	12	40	90	0.0412	0.340
8	12	45	80	0.0317	0.581
9	14	30	80	0.0430	0.478
10	14	35	90	0.0605	0.330
11	14	40	60	0.0648	0.320
12	14	45	70	0.0719	0.121
13	16	30	90	0.0711	1.018
14	16	35	80	0.0769	0.430
15	16	40	70	0.0798	0.525
16	16	45	60	0.0839	0.591

The parameters and levels were selected as per the preliminary experiments, and OA is computed by considering the number of parameters and levels. The degrees of freedom were calculated using the formulae $N(n-1)$, where N is the number of factors and n is the number of levels. The OA selection should be more than the calculated value of the degrees of freedom. MRR was calculated by dividing the thickness of the workpiece by machining time. The thickness of the specimen was 2 mm and machining time is measured in minutes. The overcut is a difference between the diameter of the tool electrode and the machined hole in millimetres [18].

Results and discussion

Entropy weighting method

The entropy approach is the best way to determine the significance of replies. The entropy method is important because it gives a quantitative framework for understanding and controlling uncertainty, complexity, and disorder in a variety of fields. Encapsulating fundamental concepts of variability and randomness allows for better decision-making, optimization, and analysis in both theoretical and practical applications. This method uses a number of steps to calculate the weight of responses. At first, a decision matrix D_{mxn} should be defined by Equation (1):

$$D_{mxn} = \begin{bmatrix} \alpha_{11} & \alpha_{12} & \alpha_{13} & \cdots & \cdots & \alpha_{1n} \\ \alpha_{21} & \alpha_{22} & \alpha_{23} & \cdots & \cdots & \alpha_{2n} \\ \alpha_{31} & \alpha_{32} & \alpha_{33} & \cdots & \cdots & \alpha_{3n} \\ \vdots & \vdots & \vdots & \ddots & \ddots & \vdots \\ \vdots & \vdots & \vdots & \ddots & \ddots & \vdots \\ \alpha_{m1} & \alpha_{m2} & \alpha_{m3} & \cdots & \cdots & \alpha_{mn} \end{bmatrix} \quad (1)$$

where α_{ij} represents the performance measure of the ith alternative (experiment number) on the jth attribute (output parameters), where m is the number of experiments and n refers to the number of output parameters (Gadakh *et al*. [11]).

Equation (2) normalizes the matrix responses:

$$\mu_{ij} = \frac{\alpha_{ij}}{\sum_{i=1}^{m} \alpha_{ij}^{2}} \qquad j = 1,2, \ldots n \quad (2)$$

where, μ_{ij} is a dimensionless value belonging to the interval [0,1] for the ith alternative and jth attribute, which indicates the normalized performance.

Equation (3) calculates the entropy value V_j:

$$V_j = -a \sum_{i=1}^{m} \mu_{ij} \ln(\mu_{ij}) \qquad j = 1,2, \ldots n \quad (3)$$

where $a = 1/\ln m$ is constant, and m is the number of alternatives.

Equation (4) calculates the degree of divergence:

$$F_j = 1 - V_j \quad (4)$$

Equation (5) could be used to calculate the weight of the jth criterion:

$$w_j = \frac{F_j}{\sum_{j=1}^{n} F_j} \quad (5)$$

Multi-objective optimization based on ratio analysis

Multi-objective optimization based on ratio analysis (MOORA), called multi-criteria or multi-attribute optimization, involves optimizing multiple competing attributes while adhering to restrictions. The MOORA approach, developed by Brauers and Zavadskas [19], is a multi-objective optimization tool that can effectively address complicated manufacturing decision-making challenges. In comparison to other multi-criteria decision-making systems, the MOORA method is straightforward and easy to implement. Because this method is based solely on simple ratio analysis, it requires the fewest mathematical calculations, which may be useful and beneficial to decision-makers who do not have a strong foundation in mathematics. Additionally, the MOORA approach has a faster computing time. Unlike other multi-criteria decision-making procedures, the MOORA method can be performed using MS Excel. The MOORA approach is highly stable for a range of decision-making situations. The MOORA technique [19-22] begins with a decision matrix comparing the performance of options based on numerous criteria.

A ratio system is created to evaluate each alternative's performance on an attribute to a denominator that represents all alternatives for that attribute. Brauers and Zavadskas [19] analysed numerous ratio systems, including total ratio and Körth ratio. They found that the square root of the sum of squares of each alternative per attribute is the best choice for this denominator. This ratio is represented by Equation (6):

$$\overset{\vee}{\alpha}_{ij} = \frac{\alpha_{ij}}{\sqrt{\sum_{i=1}^{m} \alpha_{ij}^{2}}} \quad (j = 1, 2, 3, \ldots n) \tag{6}$$

The dimensionless number α_{ij} represents the normalized performance of the i^{th} alternative on the j^{th} attribute, falling within the interval [0,1]. In multi-objective optimization, normalized performances are added while maximizing helpful qualities and deducted when minimizing non-beneficial attributes. Thus, the optimization issue becomes as presented by Equation (7):

$$q_i = \sum_{j=1}^{g} \overset{\vee}{\alpha}_{ij} - \sum_{j=g+1}^{n} \overset{\vee}{\alpha}_{ij} \tag{7}$$

In Equation (7), g represents the number of characteristics to maximize, (n-g) represent the number of attributes to minimize, and q_i represents the normalized evaluation value of the i^{th} alternative across all attributes. Certain traits may be more significant than others. Prioritizing an attribute means multiplying it by its weight (significance coefficient) [18]. When the attribute weights are considered, Equation (3) becomes Equation (8):

$$q_i = \sum_{j=1}^{g} w_j \overset{\vee}{\alpha}_{ij} - \sum_{j=g+1}^{n} w_j \overset{\vee}{\alpha}_{ij} \quad (j = 1, 2, \ldots n) \tag{8}$$

The weight of the j^{th} attribute (w_j) can be computed using the analytic hierarchy process or entropy approach.

The q_i value in the decision matrix might be positive or negative based on the sum of advantageous and non-beneficial features. An ordinal rating of q_i indicates final preference. The greatest option has the highest q_i value, while the poorest has the lowest.

The entropy-weighted MOORA approach was used to optimize MRR and overcut (OC). Equations (1) to (8) were used to calculate MOORA values and rankings, which are listed in Table 2. The attributes' weights were assigned using the entropy technique, with w_j = 0.5406 for MRR and w_j = 0.4593 for OC. The highest MOORA value is regarded as the best value and ranks first as the

optimal combination for best machining performance. As a result, the experimental run 10 has the highest MOORA value (0.1731). The 15th (0.1731) and 14th (0.1590) experimental runs are the next two best combinations. For optimal machining performance, 14 V, 35 g l^{-1} electrolyte concentration, and 90 % duty cycle can be recommended.

Table 2. *MOORA based ranking*

Exp. No	Square of output responses (α_{ij}^2)		Normalized performance (α_{ij}^2)		Highest assessment q_i	Rank
	Material removal rate	Overcut	Material removal rate	Overcut		
1	0.0008	0.3906	0.1403	0.2645	0.0759	11
2	0.0009	0.3364	0.1440	0.2814	0.0778	9
3	0.0027	0.1215	0.1384	0.2642	0.0748	12
4	0.0010	0.3226	0.1853	0.1584	0.0727	13
5	0.0010	0.3652	0.1428	0.2704	0.0772	10
6	0.0009	0.3218	0.1933	0.2225	0.1022	6
7	0.0017	0.1156	0.2722	0.1538	0.0706	14
8	0.0010	0.3371	0.2917	0.1490	0.0685	15
9	0.0018	0.2282	0.3235	0.0561	0.0258	16
10	0.0037	0.1090	0.3201	0.4740	0.1731	1
11	0.0042	0.1024	0.3460	0.2003	0.0920	7
12	0.0052	0.0145	0.3592	0.2443	0.1122	4
13	0.0051	1.0359	0.3773	0.2751	0.1264	2
14	0.0059	0.1849	0.3460	0.2003	0.0920	7
15	0.0064	0.2752	0.3592	0.2443	0.1122	4
16	0.0070	0.3490	0.3773	0.2751	0.1264	2
$\sum_{i=1}^{m} \alpha_{ij}^{2}$			4.3166	3.7340		
$-a\sum_{i=1}^{m} \mu_{ij} \ln(\mu_{ij})$			-2.144	-1.67073		
w_j			0.5406	0.4593		

Analysis of variance table for multi-objective optimization

Analysis of variance (ANOVA) was used to statistically analyse the MOORA values in order to find relevant process parameters and their contributions to the machining performance [23]. As a result, the duty cycle accounts for approximately 27.06 % of machining performance. Voltage contributes 24.15 % and electrolyte content 15.58 % to machining performance, as shown in Table 3. According to the main effect Table 4, the best combination is 16 V, 35 g l^{-1} electrolyte concentration and 60 % duty cycle. The best combination is determined considering the highest-level values of machining factors superscripted with * in Table 4.

Table 3. *ANOVA table for MOORA*

Symbol	Degrees of freedom	Sequential sum of squares	Adjusted mean square	*F*-value	Contribution, %
Voltage	3	0.0040	0.001336	1.454674	24.15
Electrolyte concentration	3	0.0026	0.000862	0.938648	15.58
Duty cycle	3	0.0045	0.001497	1.630073	27.06
Error	6	0.0055	0.000919		33.20
Total	15	0.016599	0.001107		100

Figure 4 shows the main effect plot for MOORA values and the increasing voltage trend increases the output performance. The MRR and OC improve with the rise in voltage. The workpiece used for machining is a 3D-printed specimen with high toughness and strength. In order to electrochemically dissolve it, more voltage and electrolyte concentration are required [24]. The average density of the specimen is 7.9 g cm^{-3}, and a higher electrolyte concentration is required for dissolution [25].

Table 4. *Main effects table for MOORA*

Machining factors	Signal to noise ratio for MOORA				
	LEVEL 1	LEVEL 2	LEVEL 3	LEVEL 4	Delta
Voltage	0.0753	0.0796	0.1008	0.1142*	0.0389
Electrolyte concentration	0.0763	0.1113*	0.0874	0.0826	0.0350
Duty cycle	0.0991*	0.0949	0.0653	0.0596	0.0395

*Optimal parametric combination by MOORA

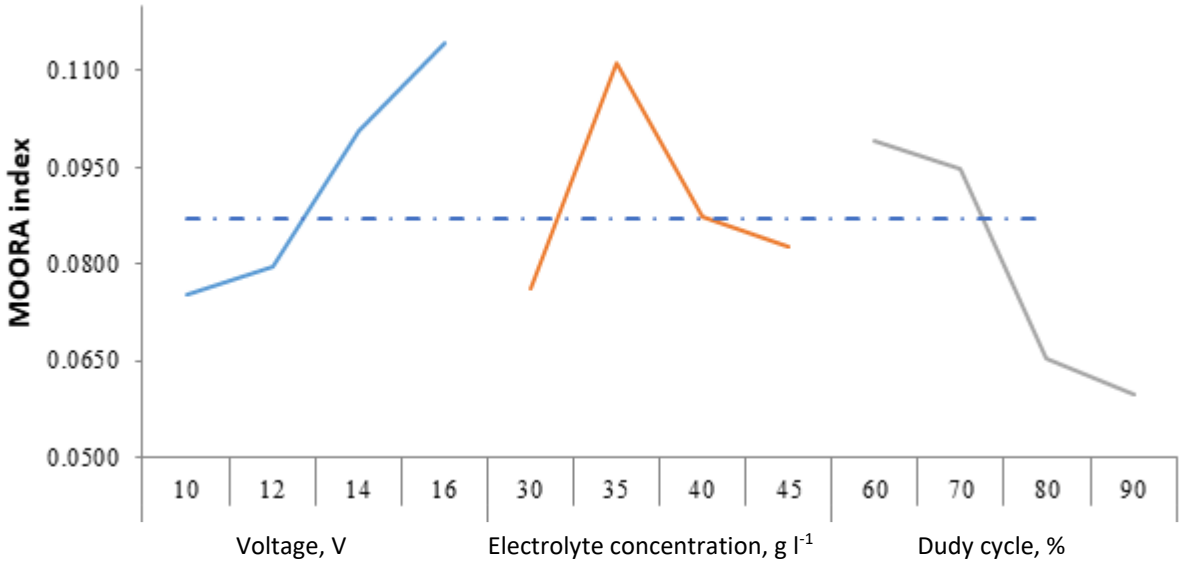

Figure 4*. Main effect plot*

Normally, in ECM, the electrolyte concentration in the 20 to 30 g l^{-1} range is sufficient for efficient machining. In this MOORA, the optimal level and main effect plot show that 35 g l^{-1} is required for machining EOS stainless steel 316L. Further increase in electrolyte concentration reduces the dissolution efficiency and accuracy. Many factors support this phenomenon, namely more hydrogen bubbles generation at the cathode, a huge mass of debris generation, and inadequate scavenging of electrolytes in the machining zone. An increase in the duty cycle has an insignificant effect on the ECM performance. The increase in duty cycle reduces the pulse-off time, which is essential for scavenging the machining zone. This short duration is insufficient for the evacuation of debris from the machining zone, leading to reduced performance.

Analysis of holes

It is evident from Figure 5 that for the hole machined at 16 V, 35 g l^{-1} of electrolyte concentration, and 60 % duty cycle, the over-etched region is witnessed around the circumference of the hole. It is due to the stray current effect on the electrode. It can be seen that the hole circumference is perfect and arresting the stray current lessens the over etched surfaces. Figure 6 shows the hole machined at ideal combinations, with no delaminated surfaces or micro-fractures observed. This phenomenon is due to the benefits of metal printing of components, which prevents future material deterioration.

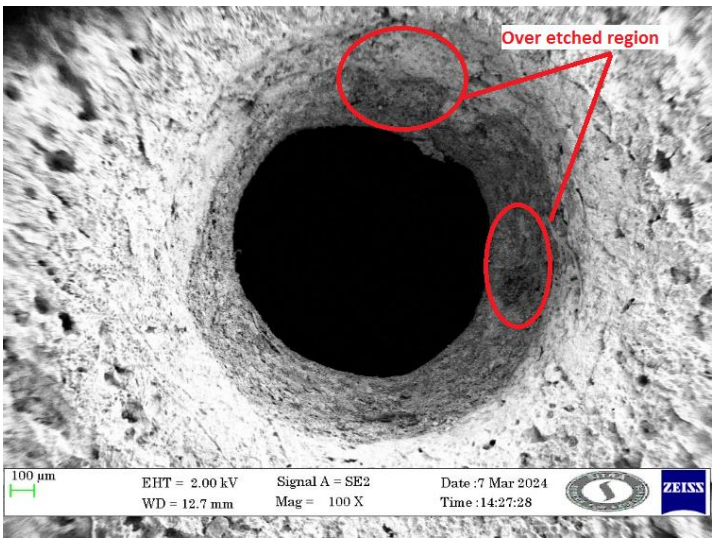

Figure 5. *Hole machined at 16 V, 35 g l^{-1} of $NaNO_3$ electrolyte concentration, and 60 % duty cycle.*

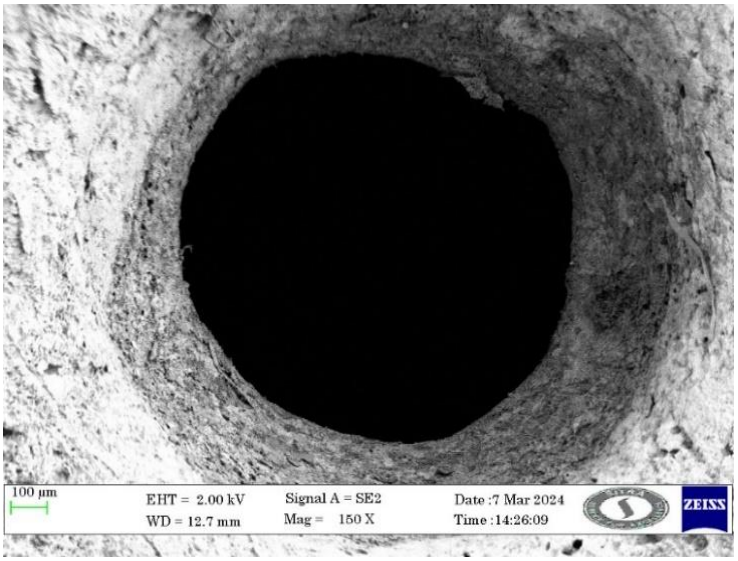

Figure 6. *Hole machined at 14 V, 35 g l^{-1} $NaNO_3$ electrolyte concentrations, and 90 % duty cycle*

Conclusions

In this experiment, the variation of ECM process variables, namely voltage, electrolyte concentration and duty cycle, are optimized with respect to material removal rate and overcut. L_{16} OA is used to conduct the experiments. The multi-criteria decision machining method, namely entropy-based multi-objective optimization based on ratio analysis (MOORA) method, is used for performance analysis. The attribute weights were assigned using the entropy technique, with w_j = 0.5406 for MRR and w_j = 0.4593 for OC. MOORA method recommends optimal machining performance as 14 V, 35 g l^{-1} $NaNO_3$ electrolyte concentration, and a 90 % duty cycle. According to the main effect table, the best combination is 16 V, 35 g l^{-1} $NaNO_3$, and 60 % duty cycle. ANOVA result shows that the duty cycle accounts for approximately 27.061 % of machining performance. Voltage contributes 24.015 %, and electrolyte content contributes roughly 15.58 % to machining performance. A scanning electron microscope was used to scan each machined hole, and different resolution images were taken in order to analyse the machined hole quality. The holes were machined at ideal combinations, with no delaminated surfaces or micro-fractures observed. This phenomenon is due to the benefits of metal printing of components, which prevents future material deterioration. Additive manufacturing technologies frequently result in materials having irregular microstructures,

porosity, and residual tensions. These irregularities can alter electrochemical reaction rates, resulting in unequal material removal. Different phases may dissolve at varying rates during ECM, resulting in localised overcutting or pitting. Microporosities and imperfections in 3D-printed materials can trap electrolytes and cause uneven dissolution. Layered structures and porosities cause non-uniform disintegration, resulting in uneven overcut profiles and low dimensional accuracy. These flaws can affect machining consistency and result in differences in MRR. Future studies can be planned to improve the hole dimensional quality.

References

[1] P. Venugopal, R. Thanigaivelan, Performance of magnetized tool in electrochemical micromachining on scrapped alloy wheel matrix composite, *Journal of Electrochemical Science and Engineering* **13(3)** (2023) 553-561. http://dx.doi.org/10.5599/jese.1660

[2] V. K. Sampath, P. Silori, P. Paradkar, S. Niauzorau, A. Sharstniou, A. Hasib, S. Villalobos, B. Azeredo, 3D printing of stainless steel 316L and its weldability for corrosive environments, *Materials Science and Engineering: A* **833** (2022) 142439. https://doi.org/10.1016/j.msea.2021.142439

[3] P. Mašek, T. Fornůsek, P. Zeman, M. Bucko, J. Smolik, P. Heinrich, Machinability the AISI 316 stainless steel after processing by various methods of 3D printing, *MM Science Journal* **November 2019** (2019) 3338-3346. http://dx.doi.org/10.17973/MMSJ.2019_11_2019091

[4] H. Zhang, J. Dang, W. Ming, X. Xu, M. Chen, Q. An, Cutting responses of additive manufactured Ti6Al4V with solid ceramic tool under dry high-speed milling processes. *Ceramics International* **46** (2020) 14536-14547. https://doi.org/10.1016/j.ceramint.2020.02.253

[5] L. Chen, Q. Xu, Y. Liu, G. Cai, J. Liu, Machinability of the laser additively manufactured Inconel 718 superalloy in turning, *International Journal of Advanced Manufacturing Technology* **114** (2021) 871-882. https://doi.org/10.1007/s00170-021-06940-8

[6] Y. Karabulut, Y. Kaynak, Drilling process and resulting surface properties of Inconel 718 alloy fabricated by selective laser melting additive manufacturing, *Procedia CIRP* **87** (2020) 355-359. https://doi.org/10.1016/j.procir.2020.02.110

[7] J. Fei, G. Liu, K. Patel, T. Özel, Effects of machining parameters on finishing additively manufactured nickel-based alloy Inconel 625, *Journal of Manufacturing and Materials Processing* **4(2)** (2020) 32. https://doi.org/10.3390/jmmp4020032

[8] Y. Bai, A. Chaudhari, H. Wang, Investigation on the microstructure and machinability of ASTM A131 steel manufactured by directed energy deposition, *Journal of Materials Processing Technology* **276** (2020) 116410. https://doi.org/10.1016/j.jmatprotec.2019.116410

[9] B. Li, R. Zhang, A. Malik, W. Li, Machinability of partition milling stainless steel/Inconel functionally gradient material printed with directed energy deposition. *The International Journal of Advanced Manufacturing Technology* **122(7)** (2022) 3009-3022. https://doi.org/10.1007/s00170-022-10111-8

[10] M. K. Ramachandran, S. A. Sumaiya, M. Golvaskar, J. Wood, I. Sluder, C. S. Rakurty, M. Kannan, Improving the Fatigue Life of an Additively Manufactured Stainless-Steel Specimen Using a Secondary Grinding Process, *Turbo Expo: Power for Land, Sea, and Air* **88018** (2024) V009T17A011. https://doi.org/10.1115/GT2024-124342

[11] V. S. Gadakh, V. B. Shinde, N. S. Khemnar, Optimization of welding process parameters using MOORA method, *The International Journal of Advanced Manufacturing Technology* **69** (2013) 2031-2039. https://doi.org/10.1007/s00170-013-5188-2

[12] A. S. Bhaskar, A. Khan, Comparative analysis of hybrid MCDM methods in material selection for dental applications, *Expert Systems with Applications* **209** (2022) 118268. https://doi.org/10.1016/j.eswa.2022.118268

[13] M. Soundarrajan, R. Thanigaivelan, Investigation of electrochemical micromachining process using ultrasonic heated electrolyte, in *Advances in Micro and Nano Manufacturing and Surface Engineering: Proceedings of AIMTDR 2018,* M. S. Shunmugam, M. Kanthababu, Eds., Springer Nature Singapore Pte LTD, 2019, 423-434. https://doi.org/10.1007/978-981-32-9425-7
[14] C. Vempannan, T. C. Kanish, D. Thirumanikandan, B. Aswin, *Electrochemical Micromachining Performance Optimization: Impact of Cathode Profile and Rotation on Machining Speed and Accuracy*, in *Advanced Manufacturing Techniques for Engineering and Engineered Materials*, R. Thanigaivelan, N. Rajan, T.G. Argul, Eds., GI Global Scientific Publishing, 2022, 20-41. https://doi.org/10.4018/978-1-7998-9574-9.ch002
[15] R. Thiraviam, V. Ravisankar, P. Kumar, R. Thanigaivelan, R. Arunachalam, A novel approach for the production and characterisation of aluminium–alumina hybrid metal matrix composites, *Materials Research Express* **7(4)** (2020) 046512. https://doi.org/10.1088/2053-1591/ab8657
[16] S. Maniraj, R. Thanigaivelan, R. Viswanathan, P. Elumalai, Experimental investigation of MRR and ROC in aluminium metal matrix composites, *Materials Today: Proceedings* **45** (2021) 1102-1106. https://doi.org/10.1016/j.matpr.2020.03.190
[17] S. Marichamy, S. Maniraj, R. Thanigaivelan, S. T. Kumaravel, K. V. Babu, P. Mallesham, Enhancement of material removal rate in EDM process using silicon carbide based strenx 900 steel, *Materials Today: Proceedings* **45** (2021) 780-782. https://doi.org/10.1016/j.matpr.2020.02.806
[18] N. Sivashankar, R. Thanigaivelan, Electrochemical micromachining of magnesium AZ31 alloy using minimum quantity electrolyte, *Materials and Manufacturing Processes* **38(11)** (2023) 1406-1415. https://doi.org/10.1080/10426914.2022.2157429
[19] W. K. M. Brauers, E. K. Zavadskas, The MOORA method and its application to privatization in a transition economy, *Control and Cybernetics* **35** (2006) 445-469. http://eudml.org/doc/209425
[20] W. K. M. Brauers, E. K. Zavadskas, Z. Turskis, T. Vilutienè, Multi-objective contractor's ranking by applying the MOORA method, *Journal of Business Economics and Management* **4** (2008) 245-255. https://doi.org/10.3846/1611-1699.2008.9.245-255
[21] D. Kalibatas, Z. Turskis, Multicriteria evaluation of inner climate by using MOORA method, *Information Technology and Control* **37** (2008) 79-83.
[22] S. Chakraborty, Applications of the MOORA method for decision making in manufacturing environment, *International Journal of Advanced Manufacturing Technology* **54(9-12)** (2011) 1155-1166. https://doi.org/10.1007/s00170-010-2972-0
[23] V.S. Gadakh, Application of MOORA method for parametric optimization of milling process, *International Journal of Applied Engineering Dindigul* **1(4)** (2011) 743-758.
[24] R. Thanigaivelan, R. M. Arunachalam, A. Nithish, S. Venkatesh, P. Naveenkumar, S. Selvaganapathy, A. S. Aravind, Optimization of Laser and Electrochemical Process Parameters for Surface Modification of Hardness and Hydrophobicity on 316L Steel*, Lasers in Engineering (Old City Publishing)* **45** (2020) 69-84. https://www.oldcitypublishing.com/journals/lie-home/lie-issue-contents/lie-volume-45-number-1-3-2020/lie-45-1-3-p-69-84/
[25] M. Shamsujjoha, S.R. Agnew, J.M. Fitz-Gerald, W.R. Moore, T.A. Newman, High strength and ductility of additively manufactured 316L stainless steel explained, *Metallurgical and Materials Transactions A* **49** (2018) 3011-3027. https://doi.org/10.1007/s11661-018-4607-2